Density Functional Calculations of *g* Values and Molybdenum Hyperfine Coupling Constants for a Series of Molybdenum(V) Oxyhalide Anions

Jacob Swann and T. David Westmoreland*

Department of Chemistry, Wesleyan University, Middletown, Connecticut 06459

Received September 6, 1996[⊗]

The electronic structures of the ions $[MoOCl_4]^-$, $[MoOF_5]^{2-}$, $[MoOCl_4(H_2O)]^-$, and $[MoOBr_4(H_2O)]^-$ have been calculated by spin-polarized density functional calculations. The results confirm and extend previous calculations on these ions. In addition, the output eigenfunctions and eigenvalues have been used to calculate *g* values and molybdenum hyperfine coupling constants. The results reproduce the trends in the experimental parameters well but tend to overestimate the magnitudes of both the *g* values and the hyperfine coupling constants. It is shown from the calculated EPR parameters that the contributions of low-energy charge transfer states and the covalencies of the ground and excited states are the major contributors to deviations of *g* values from the spin-only value. Ligand-based spin−orbit coupling becomes important with increasing atomic number for the halides but never dominates. The molybdenum hyperfine couplings are dominated by Fermi contact terms which, in turn, originate primarily from spin polarization of the core 4s electrons. A comparison of $[MoOCl_4]^-$ with $[MoOCl_4(H_2O)]^-$ indicates that the changes in EPR parameters observed on adding a sixth ligand to the coordination sphere arise from electronic structural changes due to geometrical distortions and not to specific electronic contributions from the added ligand.

Introduction

The electronic structures of complexes containing the molybdenyl ($\{MoO\}^{3+}$) group continue to be of interest largely because of their relevance to the active sites of molybdenum oxidoreductase enzymes.[1−8] Three molybdenum oxidoreductases have been crystallographically characterized: the aldehyde oxidase from *Desulfovibrio gigas*,[9] the DMSO reductase from *Rhodobacter sphaeroides*,[10] and formate dehydrogenase H from *Escherichia coli*.[11] The structural results confirm that the molybdenum atom is coordinated by the dithiolene sulfur atoms of a pterin-based cofactor,[12,13] and in the fully oxidized derivatives of the aldehyde oxidase and DMSO reductase, each molybdenum ion has at least one oxo ligand.[14] The results of extended X-ray absorption fine structure (EXAFS) spectroscopy for a number of other molybdenum oxidoreductases indicate that one or more oxo group is a common feature of the active-site structures.[15] It is also noteworthy that changes in coordination number during catalysis might be expected. The structures of the fully oxidized and fully reduced DMSO reductase indicate that the active-site molybdenum is five-coordinate in the reduced state and six-coordinate in the oxidized state.[10]

Major contributions to the understanding of molybdenum oxidoreductase active-site structures have come from electron paramagnetic resonance (EPR) spectroscopy. Partial reduction of native enzymes or treatment of the enzymes with some inhibitors produces Mo(V) species which give EPR signals in the $g \approx 2$ region. A number of these signals have been characterized in terms of *g* values and hyperfine couplings to nuclei of nonzero spin.[6,15−24] In several of these systems, anomalously high *g* values ($g_{\|} > g_e$) and/or an "inverted" trend in *g* values ($g_{\|} > g_{\perp}$) have been noted. Previous studies[25−34] of relatively simple molybdenum(V) oxyhalide anions have attributed such anomalies to various combinations of three effects: (1) large metal−ligand covalencies, (2) large values

[⊗] Abstract published in *Advance ACS Abstracts,* October 1, 1997.

(1) *Molybdenum and Molybdenum Containing Enzymes*; Coughlan, M., Ed.; Pergamon: New York, 1980.
(2) *Molybdenum Enzymes*; Spiro, T. G., Ed.; Wiley-Interscience: New York, 1985.
(3) *Molybdenum Enzymes, Cofactors, and Model Systems*; Steifel, E. I., Coucouvanis, D., Newton, W. E., Eds.; ACS Symposium Series 535; American Chemical Society: Washington, DC, 1993.
(4) Steifel, E. I. *Prog. Inorg. Chem.* **1977**, *22*, 1−223.
(5) Burgmayer, S. J. N.; Steifel, E. I. *J. Chem. Educ.* **1985**, *62*, 943−953.
(6) Bray, R. C. *Q. Rev. Biophys.* **1988**, *21*, 299−329.
(7) Wooton, J. C.; Nicolson, R. E.; Cock, J. M.; Walters, D. E.; Burke, J. F.; Doyle, W. A.; Bray, R. C. *Biochem. Biophys. Acta* **1991**, *1057*, 157−185.
(8) Enemark, J. H.; Young, C. G. *Adv. Inorg. Chem.* **1993**, *40*, 1−88.
(9) Romão, M. J.; Archer, M.; Moura, I.; Moura, J. J. G.; LeGall, J.; Engh, R.; Schneider, M.; Hof, P.; Huber, R. *Science* **1995**, *270*, 1170−1176.
(10) Schindelin, H.; Kisker, C.; Hilton, J.; Rajagopalan, K. V.; Rees, D. C. *Science* **1996**, *272*, 1615−1621.
(11) Boyington, J. C.; Gladyshev, V. N.; Khangulov, S. V.; Stadtman, T. C.; Sun, P. D. *Science* **1997**, *275*, 1305−1308.
(12) (a) Johnson, J. L.; Hainline, B. E.; Rajagopalan, K. V. *J. Biol. Chem.* **1980**, *255*, 1783−1786. (b) Rajagopalan, K. V.; Johnson, J. L. *J. Biol. Chem.* **1992**, *267*, 10199−10202. (c) Rajagopalan, K. V. In ref 3; pp 38−49.
(13) Collison, D.; Garner, C. D.; Joule, J. A. *Chem. Soc. Rev.* **1996**, 25−32.
(14) Formate dehydrogenase H contains a selenocysteine ligand rather than an oxo ligand.[11]
(15) Cramer, S. P. *Adv. Inorg. Bioinorg. Mech.* **1983**, *2*, 259−316.
(16) Barber, M. J.; Coughlan, M. P.; Rajagopalan, K. V.; Siegel, L. M. *Biochemistry* **1982**, *21*, 3561−3568.
(17) Bray, R. C.; George, G. N.; Gutteridge, S.; Norlander, L.; Stell, J. G. P.; Stubley, C. *Biochem. J.* **1982**, *203*, 263−267.
(18) Gutteridge, S.; Bray, R. C.; Notton, B. A.; Fido, R. J.; Hweitt, E. J. *Biochem. J.* **1983**, *213*, 137−142.
(19) Solomonson, L. P.; Barber, M. J.; Howard, W. D.; Johnson, J. L.; Rajagopalan, K. V. *J. Biol. Chem.* **1984**, *259*, 849−853.
(20) George, G. N.; Bray, R. C. *Biochemistry* **1988**, *27*, 3603−3609.
(21) Kay, C. J.; Barber, M. J. *Biochemistry* **1989**, *28*, 5750−5758.
(22) Bastian, N. R.; Kay, C. J.; Barber, M. J.; Rajagopalan, R. V. *J. Biol. Chem.* **1991**, *266*, 45−51.
(23) Wilson, G. L.; Greenwood, R. J.; Pilbrow, J. R.; Spence, J. T.; Wedd, A. G. *J. Am. Chem. Soc.* **1991**, *113*, 6803−6812.
(24) Dhawan, I. K.; Pacheco, A.; Enemark, J. H. *J. Am. Chem. Soc.* **1994**, *116*, 7911−7912.
(25) DeArmond, K.; Garrett, B. B.; Gutowsky, H. S. *J. Chem. Phys.* **1965**, *42*, 1019−1025.
(26) Kon, H.; Sharpless, N. E. *J. Phys. Chem.* **1966**, *70*, 105−111.
(27) Manoharan, P. T.; Rogers, M. T. *J. Chem. Phys.* **1968**, *49*, 5510−5519.
(28) Lee, G. R.; Spence, J. T. *Inorg. Chem.* **1972**, *11*, 2354−2356.

S0020-1669(96)01097-X CCC: $14.00

of ligand spin−orbit coupling, and (3) the influence of low-energy charge transfer states.

There have been a number of computational attempts to determine the relationship between experimental EPR parameters and electronic structure for a variety of transition metal complexes. Previous studies on molybdenyl complexes have tended to use bonding coefficients from separate calculations in approximate LCAO expressions for g values.[25,27,32,35] Only recently have attempts been made to calculate EPR parameters of transition metal complexes by direct evaluation of the relevant matrix elements over complete molecular wave functions.[36−38] This has been made possible by the development of reasonably reliable and efficient density functional methods for electronic structure calculations of transition metal complexes.[39]

We report herein the results of such calculations on the high-symmetry, well-characterized molybdenum(V) oxyhalide series $[MoOF_5]^{2-}$, $[MoOCl_4]^-$, $[MoOCl_4(H_2O)]^-$, and $[MoOBr_4(H_2O)]^-$. These complexes have been studied extensively by EPR[25−29,34,40−44] and optical[33,43−47] spectroscopies, and several computational studies have previously appeared.[32,48,49] Our previous work[34] suggested that the dominant contribution to the magnitudes of g values in the molybdenum oxyhalides is the metal−ligand covalencies of the ground and excited states, while inclusion of charge transfer states alone or ligand-based spin−orbit coupling plays an important but secondary role. These studies also indicated that Fermi contact interactions were the major contributors to the observed molybdenum hyperfine couplings. The methodology outlined below and in the Supporting Information provides a means of more completely defining electronic structure/EPR parameter correlations for these and other complexes. Similar computational studies have been carried out for several other transition metal complexes[36−38] but few involving fourth- or fifth-row elements and none for molybdenum-containing systems.

Table 1. Idealized Structural Parameters for Molybdenum Oxyhalide Anions[a]

complex	Mo−O	Mo−X_{eq}	Mo−L_{ax}	O−Mo−L_{eq}	ref
$[MoOCl_4]^-$	1.610	2.333		105.25	43a
$[MoOF_5]^{2-}$	1.710	1.945	1.990	95.60	50
$[MoOCl_4(H_2O)]^-$ [b]	1.672	2.359	2.393	99.00	43b
$[MoOBr_4(H_2O)]^-$ [b]	1.656	2.529	2.337	97.69	51

[a] Distances are given in angstroms, and angles are in degrees. [b] For aqua complexes, O−H = 0.98 Å and H−O−H = 107°.

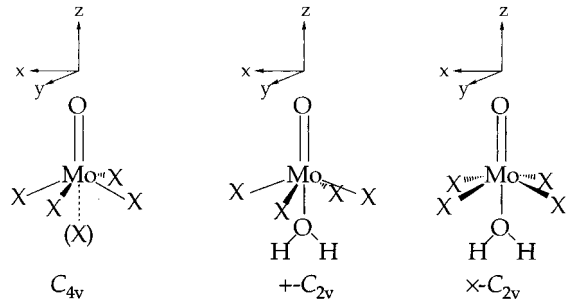

Figure 1. Definition of coordinate systems for the complexes.

Computational Methods

All molecular coordinates were based on crystallographic data for the complexes, and no geometry optimizations were performed. Experimentally determined structures were idealized to C_{4v} ($[MoOCl_4]^-$ and $[MoOF_5]^{2-}$) or C_{2v} symmetry ($[MoOX_4(H_2O)]^-$; X = Cl, Br). The final structural parameters are given in Table 1. In the case of the aqua species, the locations of the hydrogen atoms were not resolved in the X-ray data and the orientation of the water is unknown. Both the geometry with the water staggered between the halides (denoted ×-$[MoOX_4(H_2O)]^-$) and the geometry with the water eclipsed in one of the X−Mo−O planes (denoted +-$[MoOX_4(H_2O)]^-$) were considered. The coordinate systems are illustrated schematically in Figure 1.

Single-point calculations were performed using the Amsterdam Density Functional (ADF) Version 1.3.1 package of density functional routines[52,53] on an IBM RS6000 Model 550. In the ADF program, molecular orbitals are expanded in terms of Slater type orbitals (STOs) and the one-electron Kohn−Sham equations[54] are solved self-consistently using highly efficient numerical techniques.[55,56] The Vosko, Wilk, and Nusair parametrization[57] of the exchange and correlation energy of the homogeneous electron gas[58] was utilized in the local density approximation. Becke's gradient correction to the exchange part of the potential[59] and Perdew's gradient correction to the correlation[60] were included self-consistently.[61] Spin-unrestricted calculations were performed by holding all electrons in the variational space. For all atoms, triple-ζ basis sets were employed and, except for molybdenum and bromine, one polarization function was included for each atom. Polarization functions for Mo and Br have not been implemented in the currently available ADF basis sets. The unpaired

(29) (a) Radhakrishna, S.; Chowdari, B. V. R.; Viswanath, A. K. *Chem Phys. Lett.* **1975**, *30*, 231−234. (b) Radhakrishna, S.; Chowdari, B. V. R.; Viswanath, A. K. *Chem. Phys. Lett.* **1976**, *42*, 319−322.
(30) Boyd, I. W.; Dance, I. G.; Murray, K. S.; Wedd, A. G. *Aust. J. Chem.* **1978**, *31*, 279−284.
(31) Hanson, G. R.; Brunette, A. A.; McDonell, A. C; Murray, K. S.; Wedd, A. G. *J. Am. Chem. Soc.* **1981**, *103*, 1953−1959.
(32) (a) Sunil, K. K.; Harrison, J. F.; Rogers, M. T. *J. Chem. Phys.* **1982**, *76*, 3087−3097. (b) Sunil, K. K. Ph.D. Thesis, Michigan State University, 1980.
(33) Sabel, D. M.; Gewirth, A. A. *Inorg. Chem.* **1994**, *33*, 148−156.
(34) Balagopalakrishna, C.; Kimbrough, J. T.; Westmoreland, T. D. *Inorg. Chem.* **1996**, *35*, 7758−7768.
(35) Peng, G.; Nichols, J.; McCullough, E. A., Jr.; Spence, J. T. *Inorg. Chem.* **1994**, *33*, 2857−2864.
(36) Gewirth, A. A; Cohen, S. L.; Schugar, H. J.; Solomon, E. I. *Inorg. Chem.* **1987**, *26*, 1133−1146.
(37) Nogueira, S. R.; Guenzburger, D. *Int. J. Quantum Chem.* **1995**, *54*, 381−392.
(38) Belanzoni, P.; Baerends, E. J.; van Asselt, S.; Langewen, P. B. *J. Phys. Chem.* **1995**, *99*, 13094−13102.
(39) Zeigler, T. *Chem. Rev.* **1991**, *91*, 651−667 and references therein.
(40) Hare, C. R.; Bernal, I.; Gray, H. B. *Inorg. Chem.* **1962**, *1*, 831−835.
(41) (a) van Kemenade, J. T. C.; Verbeek, J. L.; Cornaz, P. F. *Recl. Trav. Chim. Pays-Bas* **1966**, *85*, 629−630. (b) van Kemenade, J. T. C. *Recl. Trav. Chim. Pays-Bas* **1970**, *89*, 1100−1108. (c) van Kemenade, J. T. C. *Recl. Trav. Chim. Pays-Bas* **1973**, *92*, 1102−1120.
(42) Dalton, L. A.; Bereman, R. D.; Brubaker, C. H., Jr. *Inorg. Chem.* **1969**, *8*, 2477−2480.
(43) (a) Garner, C. D.; Hill, L. H.; Mabbs, F. E.; McFadden, D. L.; McPhail, A. T. *J. Chem. Soc., Dalton Trans.* **1977**, 853−858. (b) Garner, C. D.; Hill, L. H.; Mabbs, F. E.; McFadden, D. L.; McPhail, A. T. *J. Chem. Soc., Dalton Trans.* **1977**, 1202−1207.
(44) Scullane, M. I.; Taylor, R. D.; Minelli, M.; Spence, J. T.; Yamanouchi, K.; Enemark, J. H.; Chasteen, N. D. *Inorg. Chem.* **1979**, *18*, 3213−3219.
(45) (a) Gray, H. B.; Hare, C. R. *Inorg. Chem.* **1962**, *1*, 363−368. (b) Winkler, J. R.; Gray, H. B. *Comments Inorg. Chem.* **1981**, *1*, 257−263.
(46) Collison, D. *J. Chem. Soc., Dalton Trans.* **1990**, 2999−3006.
(47) Carducci, M. D.; Brown, C.; Solomon, E. I.; Enemark J. H. *J. Am. Chem. Soc.* **1994**, *116*, 11856−11868.
(48) Weber, J.; Garner, C. D. *Inorg. Chem.* **1980**, *19*, 2206−2209.
(49) Deeth, R. J. *J. Chem. Soc., Dalton Trans.* **1991**, 1895−1900.
(50) Mattes, R.; Mennemann, K.; Jackel, N.; Rieskamp, H.; Brockmeyer, H. J. *J. Less-Common Met.* **1980**, *76*, 199−212.
(51) Bino, A.; Cotton, F. A. *Inorg. Chem.* **1979**, *18*, 2710−2713.
(52) Baerends, E. J.; Ellis, D. E.; Ros, P. *Chem. Phys.* **1973**, *2*, 41−51.
(53) Baerends, E. J.; Ros, P. *Int. J. Quantum Chem. Quantum Chem. Symp.* **1978**, *12*, 169−190.
(54) Kohn, W.; Sham, L. J. *Phys. Rev.* **1965**, *140*, A1133−A1138.
(55) Boerrigter, P. M.; te Velde, G.; Baerends, E. J. *Int. J. Quantum Chem.* **1988**, *33*, 87−113.
(56) te Velde, G.; Baerends, E. J. *J. Comput. Phys.* **1992**, *99*, 84−98.
(57) Vosko, S. J.; Wilk, L.; Nusair, M. *Can. J. Phys.* **1980**, *58*, 1200−1211.
(58) Ceperley, D. M.; Alder, B. J. *Phys. Rev. Lett.* **1980**, *45*, 566−569.
(59) Becke, A. D. *Phys. Rev. A* **1988**, *38*, 3098−3100.
(60) (a) Perdew, J. P. *Phys. Rev. B* **1986**, *33*, 8822−8824. (b) Perdew, J. P. *Phys. Rev. B* **1986**, *34*, 7406 (erratum).
(61) Fan, L.; Zeigler, T. *J. Chem. Phys.* **1991**, *94*, 6057−6063.

electron was arbitrarily set as α spin. The β spin MOs are nearly identical in composition and identical in ordering.

The nonzero elements of the g interaction matrix were calculated from eqs 1 and 2.[62−64] In eq 2, $|0\rangle$ is the electronic ground state wave

$$g_{ij} = g_e - \Lambda_{ij} \quad (i, j = x, y, z) \tag{1}$$

$$\Lambda_{ij} = \sum_{n\neq 0} \frac{\langle n|\xi(r)\,\hat{L}_i|0\rangle\langle 0|\hat{L}_j|n\rangle + \langle 0|\xi(r)\,\hat{L}_i|n\rangle\langle n|\hat{L}_j|0\rangle}{E_n - E_0} \tag{2}$$

function, $|n\rangle$ is an excited state, $\hat{L}_i$ and $\hat{L}_j$ are orbital angular momentum operators about the i and j axes, and $E_n - E_0$ corresponds to the excitation energy to the excited state $|n\rangle$.

The nonzero elements of the molybdenum hyperfine interaction matrix were calculated from the standard perturbation expressions[62,64] given in eqs 3−6. In eq 3, A_F is the nonclassical Fermi contact term.

$$A_{ij} = A_F + A_{ij}^{(1)} + A_{ij}^{(2)} \tag{3}$$

$$A_F = \frac{8\pi}{3} g_e g_N \beta\beta_N [|\Psi_\alpha(0)|^2 - |\Psi_\beta(0)|^2] \tag{4}$$

$$A_{ij}^{(1)} = g_e g_N \beta\beta_N \left\langle 0\left|\frac{F_{ij}}{r^3}\right|0\right\rangle \tag{5}$$

$$A_{ij}^{(2)} = g_e g_N \beta\beta_N \sum_{n\neq 0} \left[\frac{\langle 0|\xi(r)\,\hat{L}_i|n\rangle\left\langle n\left|\frac{\hat{L}_j}{r^3}\right|0\right\rangle + \langle n|\xi(r)\,\hat{L}_i|0\rangle\left\langle 0\left|\frac{\hat{L}_j}{r^3}\right|n\right\rangle}{E_n - E_0} + \frac{1}{2}\sum_{kl} i\epsilon_{kli} \frac{\langle 0|\xi(r)\,\hat{L}_k|n\rangle\left\langle n\left|\frac{F_{lj}}{r^3}\right|0\right\rangle + \langle n|\xi(r)\,\hat{L}_k|0\rangle\left\langle 0\left|\frac{F_{lj}}{r^3}\right|n\right\rangle}{E_n - E_0} \right] \tag{6}$$

$A_{ij}^{(1)}$ corresponds (for orbitally nondegenerate ground states) to the spin dipolar term, which represents the dipole−dipole coupling of the electronic spin with the spin of the nucleus. $A_{ij}^{(2)}$ is the orbital dipolar term which accounts for the coupling of the orbital angular momentum of the unpaired electron with the nuclear spin. In eqs 4−6, g_N and β_N are the values of the nuclear g factor and magneton, respectively, Ψ_α(0) and Ψ_β(0) are the values of the α and β spin total molecular wave functions, respectively, at $r = 0$, and F_{ij} is the dipolar operator, defined by

$$F_{ij} = \frac{3r_i r_j - r^2\delta_{ij}}{r^2} \tag{7}$$

in which δ_{ij} is the Dirac delta function for $i, j = x, y, z$. ϵ_{kli} is the Levi−Civita permutation symbol.[65]

In the ADF package, the molecular orbitals are expressed as expansions of STOs centered on the nuclei, and the integrands in eqs 2, 5, and 6 involve products of STOs which must be evaluated numerically. In this work, the integration scheme used was a Monte Carlo based algorithm.[66] For each matrix element, $\langle\psi_n|\hat{O}|\psi_m\rangle$, the integrand was evaluated at a particular point in space and then multiplied by an appropriate volume element generated by the integration routine. Due to the approximate nature of the integrations, it has not been assumed that the hermitian relationship $\langle\varphi_a|\hat{O}|\varphi_b\rangle = \langle\varphi_b|\hat{O}|\varphi_a\rangle^*$ is strictly valid for the calculated matrix elements of hermitian operators and eqs 2 and 6 have been retained in the form given. Additional details of the matrix element evaluation procedures are given in the Supporting Information.

Table 2. One-Electron Spin−Orbit Coupling Parameters and Atomic Charges from Mulliken Analysis[a]

complex	Mo	O	X_{eq}[b]	X'_{eq}[c]	L_{ax}	H
$[MoOCl_4]^-$	605	71	587			
	(+1.58)	(−0.69)	(−0.47)			
$[MoOF_5]^{2-}$	714	71	269		269	
	(+2.41)	(−0.87)	(−0.71)		(−0.71)	
×-$[MoOCl_4(H_2O)]^-$	587	71	587		71	0.0
	(+1.61)	(−0.65)	(−0.51)		(−0.49)	(+0.28)
+-$[MoOCl_4(H_2O)]^-$	582	71	587	587	71	0.0
	(+1.62)	(−0.60)	(−0.52)	(−0.50)	(−0.48)	(+0.27)
×-$[MoOBr_4(H_2O)]^-$	610	71	2457		71	0.0
	(+1.44)	(−0.64)	(−0.46)		(−0.50)	(+0.27)
+-$[MoOBr_4(H_2O)]^-$	610	71	2457	2457	71	0.0
	(+1.41)	(−0.62)	(−0.48)	(−0.44)	(−0.49)	(+0.26)

[a] All energies are given in cm^{-1}. Calculated atomic charges from Mulliken analysis are given in parentheses. [b] Refers in the +-C_{2v} geometry to X in the plane of the aqua ligand. [c] Refers in the +-C_{2v} geometry to X in the plane perpendicular to the aqua ligand.

Excited state wave functions were approximated by the ground state one-electron orbital of α spin corresponding to the singly occupied molecular orbital (SOMO) of the excited state. In this approximation, the effects of orbital relaxation in the excited state are completely ignored. The corresponding excited state energies were approximated by the differences in the ground state one-electron orbital energies. This approximation is better in density functional approaches than for similar Hartree−Fock calculations since in the Kohn−Sham equations the effective field for an orbital is that due to $N - 1$ electrons.[38]

In addition to quantities computed directly by ADF, spin−orbit coupling constants for all non-hydrogen atoms are required. Constants based on calculated values of $\langle r^{-3}\rangle$ proved to be unreliable for heavy atoms (particularly Br), and one-electron spin−orbit coupling parameters were taken from experimental data.[67] For the halogens, eq 8 was

$$\xi \approx \frac{2\Delta E_{JJ'}}{J(J+1) - J'(J'+1)} \tag{8}$$

used to estimate spin−orbit parameters for the oxidation state closest to that of the atom in the complex as determined by a Mulliken charge analysis. In eq 8, $\Delta E_{JJ'}$ is the experimentally observed splitting between the J and J' levels within the same (L,S) term. For the calculations presented below, ξ was taken as the average over several terms of the free ion. For oxygen, the previously reported value of ξ for $O^-(g)$ was used.[68] For the molybdenum atom, a more sophisticated parametrization which permits interpolation of values for fractional oxidation states of d^n configurations was employed.[69] Table 2 gives both the atomic charges as calculated in ADF and the one-electron spin−orbit coupling parameters used in each calculation.

Results and Analysis

Electronic Structure. Consistent with all other computational studies,[32,48,49] the ground state was found to be $^2B_2$ for the C_{4v} complexes. For ×-$[MoOX_4(H_2O)]^-$ the ground state is $^2A_1$, while for +-$[MoOX_4(H_2O)]^-$ the ground state corresponds to a $^2A_2$ representation. For each of the complexes, the electronic configuration of molybdenum is formally $4d^1$ and the unpaired electron is located in a MO of predominantly Mo $4d_{xy}$ character (formally $d_{x^2-y^2}$ for ×-C_{2v} complexes). In all cases, the SOMO is a Mo−X π^* antibonding orbital involving the halide p_x and p_y orbitals. The charge distributions in the complexes, given in Table 2, are similar to those previously calculated by discrete variational−Xα (DV−Xα) approaches.[49] While each is formally a Mo(V) complex, the effective oxidation

(62) Abragam, A.; Bleaney, B. *Electron Paramagnetic Resonance of Transition Ions*; Dover: New York, 1986.
(63) Wertz, J. E.; Bolton, J. R. *Electron Spin Resonance*; Chapman and Hall: New York, 1986. See also references therein.
(64) Mabbs, F. E.; Collison, D. *Electron Paramagnetic Resonance of d Transition Metal Compounds*; Elsevier: Amsterdam, 1992. See also references therein.
(65) Defined in, for example: Bourne, D. E.; Kendall, P. C. *Vector Analysis and Cartesian Tensors*; Chapman and Hall: New York, 1992; p 251.
(66) Petersson, G. A., Wesleyan University. Unpublished results.
(67) Moore, C. E. *Atomic Energy Levels*; National Bureau of Standards: Washington, DC, 1971.
(68) Neumark, D. M.; Lykke, K. R.; Andersen, T.; Lineberger, W. C. *Phys. Rev. A* **1985**, *32*, 1890−1892.
(69) Bendix, J.; Brorson, M., Schäffer, C. E. *Inorg. Chem.* **1993**, *32*, 2838−2849.

Table 3. Valence Orbital Compositions for $[MoOCl_4]^-$ [a]

MO	energy (eV)	Mo			O		Cl		
		% d	% p	% s	% s	% p	% s	% p	% d
$19a_1$	−0.718	42	1	16	1	23	0	10	6
$9b_1$	−1.561	53					0	42	4
15e	−2.546	59		0		24	0	15	2
$4b_2$	**−4.443**	**62**						**36**	**2**
$2a_2$	−5.680							100	0
14e	−6.272	1		1		2	−1	97	0
$8b_1$	−6.300	1					0	100	0
13e	−6.623	3		0		5	0	92	0
$18a_1$	−7.113	1	0	4	0	7	0	87	0
12e	−7.758	2		5		10	1	81	0
$17a_1$	−8.541	0	5	1	0	11	2	80	0
$3b_2$	−8.550	34						63	2
$7b_1$	−9.045	37					3	59	1
11e	−10.159	32		0		59	0	8	0
$16a_1$	−10.274	32	1	2	5	52	1	9	0
10e	−18.631	1		−1		0	100	0	0
$6b_1$	−18.643	3					98	0	0
$15a_1$	−19.093	0	0	0	0	0	98	1	0
$14a_1$	−22.994	6	−2	5	91	0	0	0	0

[a] Energies are given for the α spin MOs. Boldfaced type indicates the SOMO.

state of the metal center varies between +1.4 and +2.5 and the complexes exhibit a substantial degree of covalency. The bonding in $[MoOF_5]^{2-}$ is considerably more ionic than that in the other complexes.

As a representative example, Table 3 gives the valence orbital compositions for the $[MoOCl_4]^-$ anion from the ADF calculations. For $[MoOCl_4]^-$ (as well as each of the other complexes) there are low-lying unfilled orbitals of primarily Mo d character which correspond to ligand field excited states. The 15e orbital corresponds to the degenerate d_{xz}, d_{yz} based orbital, $9b_1$ is the $d_{x^2-y^2}$ orbital, and $19a_1$ corresponds to the d_{z^2} orbital. Just below the $4b_2$ SOMO is a set of orbitals ($17a_1$ through $2a_2$) with primarily chlorine p character which essentially correspond to lone pairs. Below these are Mo−Cl σ- and π-bonding orbitals ($7b_1$ and $3b_2$, respectively) with considerable metal and chlorine character. At even lower energy are the Mo−O bonding orbitals ($16a_1$ and 11e), three chlorine localized pairs ($15a_1$ through 10e), and an oxygen-based pair ($14a_1$). The energy orderings and orbital compositions are essentially identical to those reported by Sunil *et al.*[32] and by Deeth.[49]

Symmetry and energy constraints limit the number of orbitals which must be considered in the EPR analysis. In C_{4v} symmetry only excited states of b_1 or e symmetry are relevant. In $\times$-C_{2v} symmetry the required representations are a_2, b_1, and b_2 (which correspond to a_1, b_1, and b_2 in +-C_{2v} symmetry). Tables 4−9 summarize the orbital compositions for all the complexes but only include the orbitals important to the EPR parameter calculations. These include the SOMO (which corresponds to the ground state), empty orbitals of primarily d character (corresponding to ligand field excited states), and filled ligand-based orbitals (which correspond to charge transfer states) within 50 000 cm^{-1} of the SOMO energy. Complete tables of valence orbital compositions and energies for the complexes are given in the Supporting Information. In all cases where comparable calculations have been published,[32,48,49] the orbital energy orderings[70] and compositions match well.

The effects of an increase in coordination number on orbital energies and compositions are apparent in Tables 4−6. For all three oxychloride complexes, the SOMO characters are essentially identical. Likewise, only negligible changes are apparent in the compositions of the orbitals which make significant contributions to the EPR parameters. The orbital energies of the three complexes are comparable. The largest change is a significant drop (~4000 cm^{-1}) in the energy of the 15e orbital ($16b_1 + 16b_2$ of $[MoOCl_4(H_2O)]^-$). This decrease in energy can be rationalized in terms of the geometry differences between the five- and six-coordinate complexes. From Table 1 it is apparent that the addition of a water molecule to $[MoOCl_4]^-$ is accompanied by a decrease in the O−Mo−Cl angle of over 6°. This distortion places the chlorides more fully into the equatorial plane of the metal atom and decreases the extent of σ interaction of the chlorine orbitals with the d_{xz} and d_{yz} orbitals. The net smaller effective ligand field interaction causes the energy of these orbitals to decrease relative to the ground state. Significant differences between the species are also apparent in some of the orbitals which do not contribute to the EPR parameters and are therefore not included in Tables 4−6 (see Supporting Information). On the whole, however, binding of the sixth ligand yields only small differences in the overall electronic structure.

From Tables 5, 7, and 8 it is evident that both the SOMO and excited state orbital metal characters decrease in the order F > Cl > Br. This trend is consistent with expectations based on the electronegativities of the halides. The calculated difference in SOMO metal character between the chloride and bromide complexes is very small but is consistent with the results of both DV−Xα calculations[49] and simplified LCAO approaches.[34]

Excited State Energies. The excited states in these systems which are of importance in the calculation of EPR parameters are the one-electron ligand field excited states and ligand-to-metal charge transfer excited states. Excitation energies, as estimated by the ground state one-electron orbital energy differences, are included in Tables 4−9 for the orbitals of relevance to the EPR analysis.

In Table 10 are compared the calculated and experimentally determined energies for the excited states which have been assigned for $[MoOCl_4]^-$. Analogous tables for the other ions are included in the Supporting Information. Agreement between the calculated energy differences and experimentally observed transition energies for the ligand field states ($9b_1 \leftarrow 4b_2$ and $15e \leftarrow 4b_2$) is excellent. The $4b_2 \leftarrow 12e$ excitation lies close in energy to that observed experimentally, while the $4b_2 \leftarrow 7b_1$ excitation is calculationally found to lie 10 000 cm^{-1} higher than the experimentally assigned energy. In the case of $[MoOF_5]^{2-}$, the agreement between the calculated energies and experimental energies for the ligand field states is somewhat poorer than that for $[MoOCl_4]^-$, but the one-electron orbital energy differences provide approximate energies similar to those from previous calculations[32,48,49] which use the Slater transition method[71] (see Supporting Information). For $[MoOCl_4(H_2O)]^-$, the calculated transition energies are in good agreement with experiment. As observed experimentally, the $^2B_1$ and $^2B_2$ excited states (^2E in C_{4v}) are at lower energy than those in the five-coordinate $[MoOCl_4]^-$ anion while the $^2A_2$ excited state is nearly identical to that of $[MoOCl_4]^-$. It is important to note that, in addition to the spectroscopically observed transitions, there are, for each complex, several low-lying transitions which are predicted by the calculations. These transitions have not been observed experimentally, presumably due to their predicted small absorptivities, but have been included in the calculation of EPR parameters. The contributions to the EPR parameters from these states are, however, nearly negligible, and the EPR

(70) While the orderings and energy differences between the one-electron orbitals are nearly identical to those previously published, the absolute orbital energies differ significantly, with the ADF energies being substantially more positive. This effect is due to the negative charges of the ions, which were compensated for in other calculations by Watson spheres[32] or additional atomic potential wells.[49]

(71) Slater, J. C. *Adv. Quantum. Chem.* **1972**, *6*, 1−92.

Table 4. Orbital Compositions and Excited State Contributions to g for $[MoOCl_4]^-$

MO	type	ΔE (cm^{-1})[a]	orbital composition		$\Delta g_{\parallel}$	$\Delta g_{\perp}$
11e	CT	46 103	32% Mo d, 59% O p, 8% Cl $p_{x,y}$			0.006
$7b_1$	CT	37 122	37% Mo d, 3% Cl s, 59% Cl $p_{x,y}$, 1% Cl d		0.039	
12e	CT	26 742	2% Mo d, 5% Mo p, 10% O p, 1% Cl s, 81% Cl $p_{x,y}$			0.002
$9b_1$	LF	23 245	53% Mo d, 42% Cl $p_{x,y}$, 4% Cl d		−0.034	
13e	CT	17 586	3% Mo d, 5% O p, 92% Cl p_z			0.015
15e	LF	15 295	59% Mo d, 24% O p, 17% Cl $p_{x,y}$, 2% Cl d			−0.041
$8b_1$	CT	14 982	1% Mo d, 100% Cl p_z		0.002	
14e	CT	14 757	1% Mo d, 1% Mo p, 2% O p, −1% Cl s, 97% Cl $p_{x,y}$			0.001
$4b_2$	ground state		62% Mo d, 36% Cl p, 2% Cl d			
				Δg	0.007	−0.018
				g(calc)	2.009	1.985
				g(exp)[b]	1.9650	1.9461, 1.9474

[a] Estimated as the absolute value of the difference in calculated energy between the indicated orbital and the SOMO. [b] Reference 32b.

Table 5. Orbital Compositions and Excited State Contributions to g for ×-$[MoOCl_4(H_2O)]^-$

MO	type	ΔE (cm^{-1})[a]	orbital composition		Δg_z	Δg_y	Δg_x
$11b_2$	CT	42 541	32% Mo d, 49% O p, 11% Cl p_z, 7% H_2O				0.006
$12b_1$	CT	41 565	32% Mo d, 57% O p, 8% Cl p_z			0.006	
$8a_2$	CT	37 317	37% Mo d, 3% Cl s, 59% Cl $p_{x,y}$, 1% Cl d		0.041		
$12b_2$	CT	31 925	1% Mo d, 2% Mo p, 14% O p, 10% Cl $p_{x,y}$, 72% H_2O				0.000
$13b_1$	CT	25 733	2% Mo d, 5% Mo p, 5% O p, 1% Cl s, 87% Cl $p_{x,y}$			0.001	
$13b_2$	CT	24 371	1% Mo d, 3% Mo p, 80% Cl $p_{x,y}$, 14% H_2O				0.002
$11a_2$	LF	22 662	53% Mo d, 1% Cl s, 41% Cl $p_{x,y}$, 4% Cl d		−0.034		
$14b_1$	CT	16 795	2% Mo d, 11% O p, 87% Cl p_z			0.014	
$9a_2$	CT	16 029	100% Cl p_z		0.001		
$14b_2$	CT	15 914	1% Mo d, 9% O p, 84% Cl p_z, 5% H_2O				0.013
$15b_2$	CT	15 348	1% Mo p, 2% O p, −1% Cl s, 97% Cl $p_{x,y}$, 1% H_2O				0.001
$15b_1$	CT	15 306	1% Mo d, 2% O p, −1% Cl s, 96% Cl $p_{x,y}$			0.001	
$16b_2$	LF	11 246	60% Mo d, 26% O p, 12% Cl_z, 1% Cl d				−0.062
$10a_2$	CT	11 224	100% Cl $p_{x,y}$		0.000		
$16b_1$	LF	11 162	60% Mo d, 25% O p, 14% Cl p_z, 1% Cl d			−0.063	
$25a_1$	ground state		61% Mo d, 36% Cl p, 3% Cl d				
				Δg	0.008	−0.041	−0.040
				g(calc)	2.010	1.961	1.962
				g(exp)[b]	1.9632	1.9400	1.9400

[a] Estimated as the absolute value of the difference in calculated energy between the indicated orbital and the SOMO. [b] Reference 34.

Table 6. Orbital Compositions and Excited State Contributions to g for +-$[MoOCl_4(H_2O)]^-$

MO	type	ΔE (cm^{-1})[a]	orbital composition		Δg_z	Δg_y	Δg_x
$11b_2$	CT	42 775	32% Mo d, 49% O p, 10% Cl p_z, 1% Cl d, 7% H_2O			0.006	
$12b_1$	CT	42 203	31% Mo d, 58% O p, 9% Cl p_z				0.006
$25a_1$	CT	42 037	22% Mo d, 3% Mo s, 1% Mo p, 2% O s, 33% O p, 2% Cl s, 26% Cl $p_{x,y}$, 10% H_2O		0.000		
$26a_1$	CT	35 708	36% Mo d, 2% Cl s, 60% Cl $p_{x,y}$		0.039		
$32a_1$	LF	36 081	28% Mo d, 10% Mo s, 2% Mo p, 12% O p, −2% Cl s, 2% Cl d, 9% Cl $p_{x,y}$, 47% H_2O		0.000		
$12b_2$	CT	32 407	1% Mo d, 2% Mo p, 14% O p, 9% Cl $p_{x,y}$, 72% H_2O			0.000	
$31a_1$	LF	31 078	17% Mo d, −2% Mo s, 9% O p, 4% Cl $p_{x,y}$, 2% Cl d, 67% H_2O		0.000		
$27a_1$	CT	30 730	2% Mo s, 1% O s, 32% O p, 1% Cl s, 58% Cl $p_{x,y}$, 5% H_2O		0.001		
$13b_1$	CT	26 516	2% Mo d, 4% Mo p, 5% O p, 1% Cl s, 87% Cl $p_{x,y}$				0.001
$13b_2$	CT	24 636	1% Mo d, 3% Mo p, 1% O p, 80% Cl $p_{x,y}$, 14% H_2O			0.002	
$30a_1$	LF	22 454	53% Mo d, 40% Cl $p_{x,y}$, 3% Cl d		−0.031		
$28a_1$	CT	20 500	1% Mo d, 5% Mo p, 1% O p, 93% Cl p_z, −1% H_2O		0.000		
$14b_1$	CT	17 921	2% Mo d, 12% O p, 87% Cl p_z				0.013
$29a_1$	CT	16 385	100% Cl p_z		0.001		
$14b_2$	CT	16 305	1% Mo d, 1% Mo p, 1% O p, −1% Cl s, 98% Cl $p_{x,y}$, 1% H_2O			0.004	
$15b_1$	CT	15 723	1% Mo d, 1% Mo p, 1% O p, −1% Cl s, 99% Cl $p_{x,y}$				0.000
$15b_2$	CT	15 650	2% Mo p, 10% O p, 83% Cl p_z, 4% H_2O			0.011	
$16b_2$	LF	11 273	60% Mo d, 25% O p, 13% Cl_z, 1% Cl d			−0.063	
$16b_1$	LF	10 589	60% Mo d, 25% O p, 12% Cl $p_{x,y}$, 1% Cl d, 1% H_2O				−0.065
$6a_2$	ground state		62% Mo d, 35% Cl p, 2% Cl d				
				Δg	0.010	−0.040	−0.046
				g(calc)	2.013	1.963	1.957
				g(exp)[b]	1.9632	1.9400	1.9400

[a] Estimated as the absolute value of the difference in calculated energy between the indicated orbital and the SOMO. [b] Reference 34.

properties are dominated by spectroscopically observable excited states (see Tables 4−9).

While the excitation energies given in Tables 4−9 do not exactly match experimental values, differences between the five-coordinate $[MoOCl_4]^-$ and the six-coordinate $[MoOCl_4(H_2O)]^-$ do parallel those observed experimentally. The addition of the sixth ligand has significant effects only on the levels of e symmetry (in C_{4v}). In the C_{2v} complexes, the degeneracy of these levels is lifted to $b_1 + b_2$ and the average energy is lowered. Since these orbitals are of the correct symmetry for

Table 7. Orbital Compositions and Excited State Contributions to g for $[MoOF_5]^{2-}$

MO	type	ΔE (cm^{-1})[a]	orbital composition[b]		$\Delta g_{\|\|}$	$\Delta g_{\perp}$
$4b_1$	CT	57 709	26% Mo d, 2% F s, 72% F $p_{x,y}$		0.020	
7e	CT	51 031	28% Mo d, 21% O p, 40% F p_z, 10% F_{ax}			0.004
8e	CT	41 181	3% Mo p, 5% O p, 91% F $p_{x,y}$, 1% F_{ax}			0.000
9e	CT	36 511	1% Mo p, −1% F s, 99% F $p_{x,y}$, 1% F_{ax}			0.000
13e	LF	35 835	−88% Mo p, 2% O p, 2% F_{ax}, 195% F s, −12% F $p_{x,y}$			0.000
$5b_1$	CT	35 552	100% F p_z		0.000	
10e	CT	31 211	3% Mo d, 44% O p, 16% F p_z, 38% F_{ax}			0.002
$6b_1$	LF	29 519	48% Mo d, 30% F s, 20% F $p_{x,y}$		−0.034	
11e	CT	28 370	1% Mo d, 9% O p, 44% F p_z, 46% F_{ax}			0.004
12e	LF	8 518	67% Mo d, 21% O p, 6% F p_z, 4% F_{ax}			−0.106
$4b_2$	ground state		75% Mo d, 25% F p			
				Δg	−0.014	−0.096
				g(calc)	1.988	1.907
				g(exp)[c]	1.894	1.913

[a] Estimated as the absolute value of the difference in calculated energy between the indicated orbital and the SOMO. [b] Fluorine characters are for equatorial fluorines unless denoted F_{ax}. [c] Reference 41b.

Table 8. Orbital Compositions and Excited State Contributions to g for ×-$[MoOBr_4(H_2O)]^-$

MO	type	ΔE (cm^{-1})[a]	orbital composition		Δg_z	Δg_y	Δg_x
$20b_2$	CT	42 004	32% Mo d, 53% O p, 1% Br d, 5% Br p_z, 7% H_2O				0.009
$21b_1$	CT	40 963	30% Mo d, 62% O p, 4% Br p_z			0.009	
$21b_2$	CT	31 673	1% Mo d, 2% Mo p, 13% O p, 6% Br $p_{x,y}$, 78% H_2O				0.001
$17a_2$	CT	31 223	42% Mo d, 1% Br d, 2% Br s, 54% Br $p_{x,y}$		0.100		
$22b_1$	CT	21 246	3% Mo d, 6% Mo p, 3% O p, 1% Br s, 85% Br $p_{x,y}$			0.002	
$20a_2$	LF	21 044	50% Mo d, 3% Br d, 1% Br s, 48% Br $p_{x,y}$		−0.061		
$22b_2$	CT	19 758	2% Mo d, 4% Mo p, 1% Br s, 83% Br $p_{x,y}$, 8% H_2O				0.003
$23b_1$	CT	12 430	4% Mo d, 7% O p, 89% Br p_z			0.080	
$25b_2$	LF	12 037	61% Mo d, 27% O p, 1% Br d, 12% Br p_z, 1% H_2O				−0.082
$23b_2$	CT	11 864	2% Mo d, 7% O p, 86% Br p_z, 4% H_2O				0.072
$25b_1$	LF	11 709	59% Mo d, 26% O p, 1% Br d, 13% Br p_z, 1% H_2O			−0.085	
$18a_2$	CT	11 701	100% Br p_z		0.002		
$24b_1$	CT	11 017	1% Mo d, 1% O p, −1% Br s, 98% Br $p_{x,y}$			0.000	
$24b_2$	CT	10 897	1% Mo p, −1 Br s, 99% Br $p_{x,y}$				0.009
$19a_2$	CT	7 288	100% Br $p_{x,y}$		0.002		
$34a_1$	ground state		60% Mo d, 1% Br d, 38% Br p				
				Δg	0.043	0.006	0.012
				g(calc)	2.046	2.008	2.014
				g(exp)[b]	2.090	1.945	1.945

[a] Estimated as the absolute value of the difference in calculated energy between the indicated orbital and the SOMO. [b] Values reported for $[MoOBr_5]^{2-}$: refs 41b and 42.

π interaction with the sixth ligand, such changes are not unexpected. Thus, in terms of the orbital characters and energies, the five-coordinate $[MoOCl_4]^-$ is very similar to the two $[MoOCl_4(H_2O)]^-$ complexes. As is also evident from Tables 5 and 6, as well as Tables 8 and 9, the orientation of the aqua ligand with respect to the halides has little effect on the overall electronic structural parameters.

The trends down the halide series also reflect those observed experimentally. For the $d_{x^2-y^2}$ based ligand field transition, the energy decreases from the fluoride to the bromide as do those of the $^2B_1 \leftarrow {}^2B_2$ and ^2E (in C_{4v}) $\leftarrow {}^2B_2$ charge transfer transitions. In contrast, the calculated energy of the $^2E \leftarrow {}^2B_2$ ligand field transition increases significantly from the fluoride to the chloride and only slightly from the chloride to the bromide.

For the purpose of the current investigation of the origins of the observed trends of the EPR parameters of the molybdenum oxyhalides, the description of the electronic structures as generated by ADF appears to be sufficient. The trends revealed are consistent with all previous calculational studies and available experimental data.

Calculated *g* Values. Tables 4−9 summarize the experimentally observed and calculated g values for the series of complexes. The calculated values are significantly different from the experimentally determined values, but the general trends within the series are reproduced. Thus insights into the origin of these trends based on analysis of the calculated values are likely to be reliable. As an example, the results for $[MoOCl_4]^-$ are presented in detail.

The experimental and calculated g values for $[MoOCl_4]^-$ are given in Table 4. Both the calculated values of $g_{\|}$ and of $g_{\perp}$ are larger than the experimental values by ∼0.04. The experimentally observed inverted ordering of the g values, $g_{\|} > g_{\perp}$, is reproduced in the calculations. Also given in Table 4 is a breakdown of individual excited state orbital contributions to the calculated g values for $[MoOCl_4]^-$. The $\Delta g_{\|}$ column of Table 4 shows that three B_1 excited states fall within 50 000 cm^{-1} of the ground state: two charge transfer states and one ligand field state. The lowest lying state is a Cl → Mo charge transfer state which has not been observed experimentally in the absorption spectrum. Its contribution to $g_{\|}$ is negligible because the $8b_1$ orbital to which it corresponds is composed almost entirely of Cl $3p_z$ orbitals which have negligible overlap with the SOMO. Next lowest is a ligand field state corresponding to the metal-based $4d_{x^2-y^2}$ orbital ($9b_1$). As expected, the contribution to $g_{\|}$ is substantial because of large interaction with the ground state through spin−orbit coupling. The highest energy contributor is a charge transfer state (corresponding to $7b_1$) with significant metal character. The contribution to $g_{\|}$ from this state is larger than might be expected, and it is due to this large positive contribution that the calculated $g_{\|}$ value is larger than g_e, in contrast to the experimental result. For the calculation of $g_{\perp}$, one ligand field state and four charge transfer states are relevant. The contribution from the ligand field state

Table 9. Orbital Compositions and Excited State Contributions to g for +-$[MoOBr_4(H_2O)]^-$

MO	type	ΔE (cm^{-1})[a]	orbital composition	Δg_z	Δg_y	Δg_x
$20b_2$	CT	42 354	32% Mo d, 55% O p, 1% Br d, 6% Br p_z, 7% H_2O		0.008	
$21b_1$	CT	41 605	32% Mo d, 55% O p, 1% Br d, 6% Br p_z, 7% H_2O			0.009
$37a_1$	CT	39 900	22% Mo d, 4% Mo s, 1% Mo p, 2% O s, 41% O p, 2% Br s, 16% Br $p_{x,y}$, 13% H_2O	0.001		
$44a_1$	LF	37 452	22% Mo d, 11% Mo s, 1% Mo p, 10% O p, 2% Br d, −2% Br s, 10% Br p, 47% H_2O	0.000		
$43a_1$	LF	32 264	20% Mo d, 1% Mo p, 10% O p, 2% Br d, 7% Br $p_{x,y}$, 58% H_2O	0.000		
$21b_2$	CT	31 937	1% Mo d, 2% Mo p, 12% O p, 6% Br $p_{x,y}$, 78% H_2O		0.000	
$38a_1$	CT	31 625	41% Mo d, 2% Br s, 54% Br $p_{x,y}$	0.095		
$39a_1$	CT	27 127	1% Mo s, 1% O s, 24% O p, 1% Br s, 64% Br $p_{x,y}$, 3% H_2O	0.011		
$22b_1$	CT	22 215	3% Mo d, 6% Mo p, 3% O p, 1% Br s, 87% Br $p_{x,y}$			0.001
$42a_1$	LF	20 691	50% Mo d, 2% Br d, 47% Br $p_{x,y}$	−0.062		
$22b_2$	CT	20 182	2% Mo d, 6% Mo p, 1% Br p, 82% Br $p_{x,y}$, 10% H_2O		0.002	
$40a_1$	CT	16 261	1% Mo d, 5% Mo p, 93% Br p_z	0.000		
$23b_1$	CT	13 794	3% Mo d, 8% O p, 88% Br p_z			0.065
$41a_1$	CT	12 053	98% Br $p_{x,y}$	0.002		
$25b_2$	LF	11 840	60% Mo d, 26% O p, 1% Br d, 12% Br p_z, 1% H_2O		−0.085	
$23b_2$	CT	11 715	1% Mo d, 4% O p, 92% Br $p_{x,y}$, 2% H_2O		0.015	
$24b_2$	CT	11 576	2% Mo p, 5% O p, 92% Br p_z, 2% H_2O		0.072	
$24b_1$	CT	11 566	1% Mo p, −1% Br s, 98% Br $p_{x,y}$			0.001
$25b_1$	LF	11 086	59% Mo d, 27% O p, 1% Br d, 12% Br $p_{x,y}$, 1% H_2O			−0.085
$12a_2$	ground state		61% Mo d, 2% Br d, 37% Br p			
			Δg	0.047	0.013	−0.009
			g(calc)	2.049	1.963	1.993
			g(exp)[b]	2.090	1.945	1.945

[a] Estimated as the absolute value of the difference in calculated energy between the indicated orbital and the SOMO. [b] Values reported for $[MoOBr_5]^{2-}$: refs 41b and 42.

Table 10. Experimentally Determined and Calculated Excited State Energies for $[MoOCl_4]^-$ [a]

transition	type[b]	exptl[c]	ADF	DV−Xα[d]	MS−Xα[e]	MS−Xα[f]
$4b_2 \leftarrow 11e$	O → Mo	30 000	46 103	31 948		
$4b_2 \leftarrow 7b_1$	Cl → Mo(pσ)	27 000	37 122			
$4b_2 \leftarrow 12e$	Cl → Mo(pσ)	28 000	26 742	29 335		25 700
$9b_1 \leftarrow 4b_2$	$d_{x^2-y^2}$	23 000	23 245	22 627	25 240	23 300
$4b_2 \leftarrow 13e$	Cl → Mo(p$\pi_{\|\|}$)		17 586			23 000
$15e \leftarrow 4b_2$	$d_{xz,yz}$	15 780	15 295	16 418	17 450	15 600
$4b_2 \leftarrow 8b_1$	Cl → Mo(p$\pi_{\|\|}$)		14 982			
$4b_2 \leftarrow 14e$	Cl → Mo(p$\pi_\perp$)		14 757			18 700

[a] All energies are given in cm^{-1}. [b] pσ denotes halide p orbitals directed at Mo, p$\pi_{\|\|}$ denotes those roughly parallel to the Mo−O bond, and p$\pi_\perp$ denotes halide p orbitals perpendicular to both p$\pi_{\|\|}$ and pσ. [c] References 33 and 47. [d] Reference 49. [e] Reference 32. [f] Reference 48.

Table 11. Effects of Metal−Ligand Covalency, Ligand Spin−Orbit Coupling, and Low-Lying Charge Transfer Excited States on Calculated g Values

	$[MoOCl_4]^-$	×-$[MoOCl_4(H_2O)]^-$	+-$[MoOCl_4(H_2O)]^-$	$[MoOF_5]^{2-}$	×-$[MoOBr_4(H_2O)]^-$	+-$[MoOBr_4(H_2O)]^-$
g_z(calc)	2.009	2.010	2.013	1.988	2.046	2.049
Mo only	1.978	1.977	1.991	1.986	1.982	1.981
$\xi_L = 0$	2.004	2.005	2.006	1.986	2.014	2.013
no CT	1.968	1.968	1.971	1.968	1.941	1.941
g_y(calc)	1.985	1.961	1.963	1.907	2.008	1.963
Mo only	1.959	1.944	1.943	1.888	1.949	1.949
$\xi_L = 0$	1.974	1.955	1.956	1.908	1.960	1.962
no CT	1.961	1.939	1.939	1.896	1.918	1.917
g_x(calc)		1.962	1.957		2.014	1.993
Mo only		1.943	1.939		1.948	1.946
$\xi_L = 0$		1.956	1.953		1.963	1.960
no CT		1.940	1.937		1.920	1.960

is largest but is significantly quenched by the charge transfer state contributions. The results are qualitatively in agreement with the experiments in that $g_\perp$ is less than $g_{||}$ and less than g_e.

Previous studies[25−34] have suggested that the three dominant factors contributing to g values in the molybdenum oxyhalides are (1) the metal−ligand covalencies of the ground and excited state orbitals, (2) ligand-based spin−orbit coupling, and (3) mixing of low-lying charge transfer excited states into the ground state. The ADF calculations provide a means of quantitatively probing these effects. In Table 11, the "Mo only" entries refer to calculated EPR parameters with the integrals evaluated only over molybdenum basis functions and correspond to neglect of ligand orbital contributions (and thus most of the effects of metal−ligand covalency[72]) in the wave functions. For $[MoOCl_4]^-$ under the "Mo only" approximation, the ligand-field state contribution is essentially unaffected, while the charge transfer contributions almost vanish, giving significantly smaller values of $g_{||}$ and $g_\perp$. The results of calculations with the chlorine spin−orbit coupling constant set to zero are given as the "$\xi_L = 0$" entry. Both the ligand field and the charge transfer state contributions decrease in magnitude. A slightly larger decrease in the charge transfer contribution results in an overall small

(72) The values do not reflect *complete* neglect of covalency since the overall metal character remains less than unity. This level of approximation is essentially equivalent to a ligand field approach incorporating orbital reduction factors.[62−64]

decrease in both $g_{\|}$ and $g_{\perp}$. The influence of charge transfer excited states is apparent in the "no CT" entries of Table 11, which give the calculated g values without the charge transfer contributions. Since the charge transfer states provide net positive contributions to the g values, it is not surprising that both $g_{\|}$ and $g_{\perp}$ are dramatically smaller. It is also notable that, in the absence of charge transfer contributions, the calculated g values become nearly isotropic. From this analysis, the charge transfer contributions are predicted to have the single largest effect on the calculated g values with metal−ligand covalency being nearly as important. Chlorine spin−orbit coupling in $[MoOCl_4]^-$ is calculated to be the smallest of the three effects.

Effects of Coordination Number: $[MoOCl_4]^-$ and $[MoOCl_4(H_2O)]^-$. Also presented in Tables 5, 6, and 11 are the calculated g value analyses for both geometries of $[MoOCl_4(H_2O)]^-$. Upon coordination of water, the experimentally determined values show a very slight drop in both $g_{\|}$ and $g_{\perp}$. For both of the aqua geometries, the calculated values exhibit a similar decrease in g_x and g_y (relative to $g_{\perp}$ for $[MoOCl_4]^-$) but a slight increase in g_z. The experimentally determined and the calculated g values, however, are very similar for both the five- and six-coordinate species. The orientation of the water in the aqua species has only a minimal effect on the g values.

The individual excited state contributions to g_z for the complexes (Tables 5 and 6) are nearly identical in both the five- and six-coordinate complexes. The effects of ignoring ligand-based contributions to the orbitals, ligand spin−orbit coupling, or charge transfer contributions (see Table 11) closely parallel those for $[MoOCl_4]^-$. As was noted above, for the states relevant to g_x and g_y, the only significant difference between the five- and six-coordinate complexes is that the lowest ligand field excited state is significantly lower in energy in the aqua complexes. The smaller energy denominator in the perturbation expressions results in slightly larger ligand field contributions to g_x and g_y. The effects of ignoring ligand-based contributions, ligand spin−orbit coupling, or charge transfer contributions also parallel those calculated for $[MoOCl_4]^-$.

Overall, the relative differences between the g values as calculated for $[MoOCl_4]^-$ and $[MoOCl_4(H_2O)]^-$ are in good agreement with experiment. The only factor which varies significantly with the presence or absence of the sixth ligand is the contribution of the lowest ligand field state(s), corresponding to the d_{xz}, d_{yz} set, to $g_{\perp}$. The change in this contribution lies almost exclusively in the difference between the transition energies for this state for the five- and six-coordinate complexes. The difference in energy can be rationalized in terms of the geometric distortions which accompany the change in coordination geometry, as described above.

The Halide Series: $[MoOF_5]^{2-}$, ×-$[MoOCl_4(H_2O)]^-$, and ×-$[MoOBr_4(H_2O)]^-$. Presented in Tables 7−9 are the calculated and experimental g values for the six-coordinate complexes $[MoOF_5]^{2-}$ and $[MoOBr_4(H_2O)]^-$. The calculated values reproduce the experimentally observed trend $g(F) < g(Cl) < g(Br)$ for both $g_{\|}$ (g_z) and $g_{\perp}$ (g_x, g_y). For all three complexes, however, the calculated ordering of $g_{\|}$ and $g_{\perp}$ is inverted while experimentally only the bromide and the chloride exhibit this feature. Also, with the exception of $g_{\perp}$ for $[MoOF_5]^{2-}$, all the calculated g values are larger than the experimentally observed values.

Upon comparison of the results in Tables 7, 5, and 8 for $[MoOF_5]^{2-}$, ×-$[MoOCl_4(H_2O)]^-$, and ×-$[MoOBr_4(H_2O)]^-$, it is apparent that the magnitude of the ligand field contributions to the g values increases modestly down the series. This effect can be attributed almost entirely to the increasing metal−halide covalency of the ligand field excited state orbitals since the variation in the calculated energies of these orbitals is relatively small. In contrast, charge transfer contributions increase dramatically down the series. This is due not only to the increasing covalency of the orbitals but also to the decrease in charge transfer excited state energies which results in greater mixing into the ground state. The trend is, therefore, that as covalency increases or charge transfer energies become smaller, the g values increase. Similar trends are evident in the results for the +-$[MoOX_4(H_2O)]^-$ geometries.

Table 11 quantitatively summarizes the effects of ligand-based orbital contributions, ligand spin−orbit coupling, and charge transfer states on the calculated g values. In all cases, neglect of ligand contributions results in a decrease in the calculated g values and the magnitude of the change becomes larger as the ligand characters of the ground and excited state orbitals increase. The effect of ligand spin−orbit coupling is nearly negligible for the fluoride complex but for the bromide complex is similar in magnitude to the covalency contribution. The largest effect on the calculated g values in each case is observed on eliminating the charge transfer contributions, and the magnitude of the change increases down the series.

Molybdenum Hyperfine Couplings. The results of the A^{Mo} calculations are given in Table 12 along with the experimentally observed parameters. While in every case the calculated magnitude is smaller than the observed, the trends in the calculated A^{Mo} values reproduce the observed experimental trends. A comparison of the five-coordinate $[MoOCl_4]^-$ anion with the six-coordinate $[MoOCl_4(H_2O)]^-$ ion shows a significant decrease in the magnitude of the calculated $A_{\|}^{Mo}$ and $A_{\perp}^{Mo}$ values. For the six-coordinate species, all A^{Mo} values decrease systematically from the fluoride to the bromide. In all cases, $A_{\|}^{Mo}$ is roughly twice the magnitude of $A_{\perp}^{Mo}$. The calculated $\langle A^{Mo}\rangle$ values parallel the observed trends but differ consistently from experimental values by approximately 15×10^{-4} cm^{-1}.

Partitioning of A^{Mo}. Experimentally measured hyperfine coupling constants represent the net total of contributions from three principal mechanisms.[62,64,73] Fermi contact, A_F, is a completely isotropic nonclassical contribution which is proportional to the unpaired spin density at the nucleus. $A^{(1)}$ represents the spin dipolar contribution and corresponds to the first-order energy of interaction due to the completely anisotropic dipole−dipole coupling of the electronic spin with the nuclear spin. The orbital dipolar term, $A^{(2)}$, is the second-order cross-term of the dipolar operator with the spin−orbit coupling operator. For a nondegenerate ground state, this contribution physically corresponds to the coupling of the net ground state orbital angular momentum to the nuclear spin. $A^{(2)}$ has both anisotropic and isotropic components. Table 12 includes the calculated contributions from each term to the total A^{Mo} values.

Fermi contact dominates the observed[34] and calculated molybdenum hyperfine structure and is chiefly responsible for the large decrease in A^{Mo} down the halide series. The spin dipolar terms are next in magnitude and likewise decrease down the halide series. Least significant are the orbital dipolar terms which parallel the calculated values of Δg and increase in magnitude somewhat down the halide series. These results agree with a previous study[34] which attributes the large difference between $A_{\|}^{Mo}$ and $A_{\perp}^{Mo}$ to relatively large spin dipolar terms. Due to the small orbital dipolar contributions and the complete anisotropy of the spin dipolar term, the average molybdenum hyperfine splittings, $\langle A^{Mo}\rangle$, are dominated by the Fermi contact.

Comparison of the molybdenum hyperfine analysis for the five- and six-coordinate chloride species shows that the most

(73) Solomon, E. I. *Comments Inorg. Chem.* **1984**, *3*, 225−320.

Table 12. Contributions to Calculated A^{Mo} Terms for Molybdenum Oxyhalide Anions[a]

	$[MoOCl_4]^-$	×-$[MoOCl_4(H_2O)]^-$	+-$[MoOCl_4(H_2O)]^-$	$[MoOF_5]^{2-}$	×-$[MoOBr_4(H_2O)]^-$	+-$[MoOBr_4(H_2O)]^-$
exp ref	43a	34	34	41c	41b, 42[b]	41b, 42[b]
A_z^{Mo}(calc)	−53.38	−45.62	−37.76	−60.02	−39.46	−30.76
A_z^{Mo}(exp)	83.19	74.7	74.7	90.1	66.0	66.0
A_y^{Mo}(calc)	−25.13	−17.44	−9.79	−23.98	−13.93	−4.30
A_y^{Mo}(exp)	37.75	32.6	32.6	42.5	30.0	30.0
A_x^{Mo}(calc)	−25.13	−17.01	−8.18	−23.98	−14.12	−3.13
A_x^{Mo}(exp)	37.75	32.6	32.6	42.5	30.0	30.0
⟨A⟩(calc)	−34.55	−26.69	−18.58	−35.99	−22.50	12.73
⟨A⟩(exp)	52.90	46.6	46.6	58.4	42.0	42.0
A_F	−37.33	−29.63	−21.60	−41.15	−26.57	−17.15
$A_z^{(1)}$	−19.80	−18.86	−18.94	−25.39	−17.54	−18.49
$A_y^{(1)}$	10.53	9.86	9.55	12.49	9.43	9.58
$A_x^{(1)}$	10.53	9.00	9.60	12.49	7.99	8.89
$A_z^{(2)}$	3.75	2.87	2.78	6.52	4.65	4.88
$A_y^{(2)}$	1.67	2.33	2.26	4.68	3.21	3.27
$A_x^{(2)}$	1.67	3.62	3.82	4.68	4.46	5.13

[a] All values in units of 10^{-4} cm^{-1}. [b] Values given are those reported for $[MoOBr_5]^{2-}$.

significant difference is in the Fermi contact terms. In addition, the rather surprising difference in A^{Mo} between the two alternative aqua geometries lies almost exclusively in the Fermi contact term. Thus, the sensitivity of the molybdenum hyperfine coupling constants to coordination environment seems to originate primarily in the Fermi contact contribution. The excited state contributions to A^{Mo} appear only in the orbital dipolar terms and parallel those of the g values. Since these terms are only minor contributors to the overall hyperfine coupling, they will not be considered further, except to note that the largest contributions to $A^{(2)}$ are from the ligand field and charge transfer states with large molybdenum d characters.

Fermi Contact. There are two principal mechanisms for Fermi contact interactions.[62,64,73] Direct contact arises from net spin density at the nucleus due to s orbital character in the ground state wave function, while indirect contact reflects the spin polarization of valence or core electrons by the unpaired valence electron to give a net excess spin density at the nucleus. For each complex with the C_{4v} or +-C_{2v} geometry, the ground state does not correspond to a totally symmetric representation in the point group of the ion. Thus, any direct Fermi contact contribution for the metal is precluded by symmetry considerations. For both of the ×-C_{2v} complexes, the a_1 ground state SOMO character is entirely Mo 4d and X *n*p and the direct Fermi contact is negligibly small. Thus, significant Fermi contact in all the complexes must be entirely indirect, arising from polarization of valence and core electrons. Symmetry considerations also require for these complexes that any indirect Fermi contact terms arise from totally symmetric molecular orbitals since all other orbitals have nodes at the metal nucleus. Table 13 presents the contributions from core and valence orbitals to the Fermi contact term both for the free Mo(V) ion and for the complexes under consideration. A detailed breakdown of the individual valence orbital contributions is given in the Supporting Information.

As noted above, the calculated values of A_F decrease down the halide series. This trend is expected since the decrease in metal character in the SOMO will decrease the extent to which the unpaired electron polarizes the core orbitals on the metal. It is clear from the calculated values in Table 13 that the major contribution to the Fermi contact in all species is the polarization of the core orbitals (particularly 4s) which yields a large, negative contribution to A_F. The magnitude varies with the extent of delocalization of the SOMO unpaired electron. The valence term is smaller and is positive for all but the fluoride complex.

Table 13. Indirect Fermi Contact Contributions to A^{Mo}

	10^{-4} cm^{-1}				%	O−Mo−X
	A_F	core[a]	4s	valence	Mo	(deg)
free ion Mo(V)	−78.1	−78.1	−68.1		100	
pentacoordinated						
$[MoOCl_4]^-$	−37.3	−40.9	−38.3	+3.6	62	105.25
"×-*[MoOCl$_4$(−)]$^-$*"[b]	−23.3	−25.1	−22.1	+1.8	63	99
"+-*[MoOCl$_4$(−)]$^-$*"[b]	−22.9	−26.0	−22.2	+3.1	63	99
"*[MoOF$_4$(−)]$^-$*"[b]	−41.3	−41.2	−40.1	−0.1	73	95.6
hexacoordinated						
$[MoOF_5]^{2-}$	−41.1	−40.0	−38.9	−1.1	75	95.6
+-$[MoOCl_4(H_2O)]^-$	−21.5	−25.0	−22.5	+3.5	62	99
×-$[MoOCl_4(H_2O)]^-$	−29.7	−36.9	−33.8	+7.2	61	99
"+-*[MoOCl$_4$(**H$_2$O**)]$^-$*"[b]	−38.3	−32.3	−29.2	−6.0	67	105.25
"×-*[MoOCl$_4$(**H$_2$O**)]$^-$*"[b]	−45.8	−50.4	−46.4	+4.5	63	105.25
+-$[MoOBr_4(H_2O)]^-$	−17.0	−21.0	−17.9	+4.0	61	97.69
×-$[MoOBr_4(H_2O)]^-$	−26.5	−32.2	−28.5	+5.7	60	97.69

[a] Core includes orbitals through Mo 4s. [b] See text for definition.

In comparing $[MoOCl_4]^-$ to the $[MoOCl_4(H_2O)]^-$ ions, a significant decrease is calculated in the A_F term. While the calculated g values are very similar for the complexes, the calculated hyperfine splittings differ by $(5-15) \times 10^{-4}$ cm^{-1}, depending on the orientation of the water molecule. These changes could be attributed either to the direct electronic effects of the sixth ligand or to geometric distortions, primarily the decrease of the O−Mo−Cl angle relative to the five-coordinate complex.

In order to investigate more thoroughly the origin of the differences in A_F between the five- and six-coordinate species, calculations were performed on several "model" ions, *i.e.*, complexes with geometries different from those observed crystallographically. Table 13 includes results for three model ions: (1) the aqua chloride species with the water ligand removed, resulting in a flattened $[MoOCl_4]^-$ geometry (denoted "*[MoOCl$_4$(−)]$^-$*"); (2) the observed $[MoOCl_4]^-$ geometry but with water added as a sixth ligand (denoted "*[MoOCl$_4$(**H$_2$O**)]$^-$*"); and (3) the $[MoOF_5]^{2-}$ geometry in the absence of the axial fluoride "*[MoOF$_4$(−)]$^-$*".

Comparing A_F for *[MoOCl$_4$(−)]$^-$* with those of the two $[MoOCl_4(H_2O)]^-$ species, little change is apparent. The differences in A_F for the ×-C_{2v} and +-C_{2v} structures for the most

part disappear, and the resulting contact term is much closer to that of the aqua species than to that of $[MoOCl_4]^-$. These results are also consistent with calculations using the observed $[MoOCl_4]^-$ geometry but with a water molecule coordinated ("*[MoOCl$_4$(**H$_2$O**)]$^-$*"). When A_F values from both of these model geometries are compared to A_F for $[MoOCl_4]^-$, a modest increase in the Fermi contact term is observed upon the addition of the sixth ligand. The A_F value for "*[MoOF$_4$(−)]$^-$*" is essentially identical to that for the six-coordinate species. Overall, these results suggest that the differences between the pentacoordinated and the hexacoordinated species arise primarily from changes in electronic structure due to geometric distortion of the $\{MoOX_4^-\}$ moiety rather than from specific axial ligand electronic effects. Similar conclusions have been reached for $[M(CN)_5]^{3-}$ (M = Co, Rh, Ir) species in terms of the effects of small changes in the $C_{ax}-M-C_{eq}$ bond angles on the Fermi contact term.[37]

The origin of the large differences in A_F between the aqua species with the same halides but different orientations of the water remains unclear. It is, however, apparent that for similar geometries A_F is dominated by polarization of the 4s shell and is correlated with the ground state metal character of the SOMO. A_F is very sensitive to the geometry, primarily the $L_{ax}-Mo-L_{eq}$ angle, and appears to be somewhat sensitive to the orientation of the aqua ligand.

Conclusions

The calculations presented above provide insight into the origins of the relative magnitudes of the EPR parameters for a series of closely related complexes. The calculated values do not, however, provide accurate estimates of the experimentally determined g and A^{Mo} values. A close inspection of the results of the calculations suggests a number of reasons for these discrepancies. The ADF calculations, like many density functional approaches to transition metal complexes, tend to overestimate covalency.[74] For example, while the ground and excited state orbital metal characters in Tables 4−9 are similar to those calculated in other density functional schemes,[32,48,49] they are all significantly smaller than those suggested by fitting the observed EPR parameters to a simplified model with adjustable bonding parameters.[34] To a significant extent, the overestimation of covalency must reflect the inadequacy of the available basis sets, particularly with respect to polarization functions. The large covalencies also affect the calculated energies of the charge transfer states and thus the perturbation expressions which are particularly sensitive to these energies. In addition, for more accurate calculation of Fermi contact terms, better all-electron basis sets will need to be developed.

The deficiencies in the basis sets are, however, systematic. It would thus be expected that while the experimentally observed EPR parameters will not be accurately reproduced, the trends in the parameters for a series of related complexes should be reasonably reflected in the calculated values. As described in the analysis above, the calculated values do reproduce the experimentally observed trends. Thus the calculations can provide insights into the origins of the observed EPR parameters if interpreted within a context of closely related compounds.

The calculations and analysis yield a number of general conclusions regarding the EPR parameters of molybdenum oxyhalide anions. In all cases, the g values are substantially sensitive to metal−ligand covalency in the ground and excited state orbitals and to the influence of low-lying charge transfer excited states. The overestimation of covalency and the underestimation of charge transfer energies lead to $g_{\parallel} > g_e$ for all the complexes, a result which is only experimentally observed for the bromide complex. The observed trend in $g_{\parallel}$ (Br > Cl > F) is, however, reproduced and can be attributed to the increased metal−halide covalencies and lower charge transfer excited state energies down the series. Ligand spin−orbit coupling becomes more important as ξ_L increases, but in no case is it the dominant contribution to the overall g values. The A^{Mo} values are dominated by Fermi contact contributions, while their anisotropies are determined almost entirely by the first-order spin dipolar coupling. The largest contribution to the Fermi contact comes from polarization of the 4s core electrons. The calculated sign of A^{Mo} is negative, and both the Fermi contact and the dipolar coupling decrease in magnitude with increasing SOMO covalency.

Addition of a sixth ligand to a five-coordinate complex results in a decrease in the magnitudes of the A^{Mo} values but nearly identical g values. The results of the calculations indicate that this is the result of the changes in geometry due to the coordination of the sixth ligand and not to specific electronic effects of the ligand. This conclusion is consistent with the experimental observation that, for a wide range of L, the EPR parameters of $[MoOCl_4L]^-$ are relatively insensitive to the specific identity of L.[75]

The conclusions presented above are consistent with the results of fitting observed EPR parameters to a much simpler LCAO model.[34] The fitting approach, however, suggested that ground and excited state covalencies were more important than the contributions of charge transfer states. A comparison of the studies suggests that the density functional based calculations seriously overestimate the contributions of low-lying charge transfer excited states. The calculational approach presented in this work does, however, provide some advantages over the simpler models. In particular, the previously described LCAO model[34] required independent measurement or estimation of excited state energies, overlap integrals, and spin−orbit coupling constants. The only external parameters required in the current approach are the spin−orbit coupling constants. In addition, simpler models are limited to relatively high-symmetry (at least C_{4v}) systems to keep the number of adjustable variables manageable. The calculational approach described above is easily extended to systems of low or no symmetry.

Acknowledgment. Prof. G. A. Petersson is acknowledged for providing computational facilities and for helpful discussions. Prof. S. E. Novick is also acknowledged for helpful discussions.

Supporting Information Available: Text giving details of matrix element evaluation methods and tables comparing selected calculated matrix elements to their analytical values, calculated valence orbital energies and compositions and experimentally assigned excited state energies for $[MoOF_5]^{2-}$, $[MoOCl_4(H_2O)]^-$, and $[MoOBr_4(H_2O)]^-$, and individual valence orbital contributions to the Fermi contact for all species (20 pages). Ordering information is given on any current masthead page.

IC961097M

(74) In a previous Xα−SW approach to copper(II) complexes,[36] adjustable sphere sizes were employed to minimize these effects.

(75) Boorman, P. M.; Garner, C. D.; Mabbs, F. E. *Chem. Soc., Dalton Trans.* **1975**, 1299−1306.